Received: 9 August 2020 | Revised: 11 January 2021 | Accepted: 3 February 2021

DOI: 10.1002/er.6586

SPECIAL ISSUE SHORT COMMUNICATION

INTERNATIONAL JOURNAL OF ENERGY RESEARCH WILEY

Effect of nickel on combustion synthesized copper/fumed-SiO_2 catalyst for selective reduction of CO_2 to CO

Anand Kumar | **Ahmed A. A. Mohammed** | **Mohammed A. H. S. Saad** | **Mohammed J. Al-Marri**

Department of Chemical Engineering, College of Engineering, Qatar University, Doha, Qatar

Correspondence
Anand Kumar, Department of Chemical Engineering, College of Engineering, Qatar University, P.O. Box 2713, Doha, Qatar.
Email: akumar@qu.edu.qa

Funding information
Qatar National Research Fund, Grant/Award Number: NPRP8-509-2-209

Summary

In this study, we explore the effect of nickel incorporation in Cu/fumed-SiO_2 catalyst for CO_2 reduction reaction. Two catalysts, Cu and CuNi supported on fumed silica were synthesized using a novel surface restricted combustion synthesis technique, where the combustion reaction takes place on the surface of the inert fumed-SiO_2 support. An active solution consisting of a known amount of metal nitrate precursors and urea (fuel) was impregnated on fumed silica. The catalyst loading was limited to 1 wt% to ensure localized combustions on the surface of fumed-SiO_2 by restricting the combustion energy density. The synthesized catalysts were tested for CO_2 hydrogenation reaction using a tubular packed bed reactor between temperature 50°C and 650°C, where Cu/SiO_2 showed high CO_2 conversion to carbon monoxide, and the addition of Ni further improved the catalytic performance and showed some tendency for methane formation along with CO. Moreover, both the catalysts were highly stable under the reaction conditions and did not show any sign of deactivation for ~42 hours time on stream (TOS). The catalysts were characterized using X-ray diffractometer (XRD), scanning electron microscope/energy dispersive X-ray spectrometer (SEM/EDX), transmission electron microscope (TEM), and the Brunauer-Emmet-Teller (BET) surface area measurement technique to understand their structural properties and to assess the effect of CO_2 conversion reaction. In situ DRIFTS was also used to investigate the reaction pathway followed on the surface of the catalysts.

KEYWORDS

carbon dioxide conversion, CO_2 hydrogenation, copper-nickel catalysts, fumed-SiO_2, surface restricted combustion synthesis

1 | INTRODUCTION

The global energy demand has surged over the past decades and is expected to continuously grow in the near future to fulfill the demand generated by continuous improvement in human life quality. So far, most of the energy is produced from fossil fuel-based sources that emit carbon dioxide (CO_2) as a byproduct during energy generation process, which is known to adversely affect the global climate.[1,2] A high concentration of CO_2 in the

atmosphere is directly linked to global temperature rise.[2] Being a thermodynamically stable molecule CO_2 can be captured and stored underground for a long time, or it can be utilized for producing commodity chemicals as a way of recycling CO_2 and reducing the overall global impact of their release into the atmosphere. While many groups are working on CO_2 capture and sequestration aspects, leading to industrial applications such as enhanced oil recovery etc.[3,4]; more efforts are required in converting CO_2 into other carbon-containing products. Utilizing CO_2 for the production of chemicals and fuels seems a sustainable approach, though it requires considerable energy at this stage on account of the relatively inert nature of the CO_2 molecule. However, it is anticipated that the renewable energy will become cheaply available in the future, which will make the cost of CO_2 conversion to fuels and chemicals drop drastically. Catalysts play a critical role in lowering the energy barrier for CO_2 conversion reactions. A suitable catalyst can bring the energy requirement to a cost-competitive stage while selectively producing the desired products. Efforts in the direction of photo-catalysis,[5,6] electro-catalysis,[7-13] and thermal catalysis[14-18] are underway, each having its advantages and disadvantages. Nonetheless, the thermal catalysis route seems more favorable for hydrocarbon reforming industries as high-pressure CO_2 streams can be easily processed within the reforming facilities while simultaneously utilizing the excess heat for an overall energy-efficient conversion process. The reduction of CO_2 in presence of H_2 can follow reverse water-gas shift (RWGS)[19] or further proceed to methanation as shown below[20-23]:

$$CO_2 + H_2 \rightarrow CO + H_2O \quad \Delta_r H^0_{298K} = 41\,\text{kJ/mol}, \quad (1)$$

$$CO + 3H_2 \rightarrow CH_4 + H_2O \quad \Delta_r H^0_{298K} = -206\,\text{kJ/mol}. \quad (2)$$

The choice of catalyst plays a crucial part in the conversion of CO_2 as there are clear evidences that the reaction pathway may follow methane formation via intermediate CO generation, or in some cases, CO generation can be completely avoided.[14,19,23] It is also clear that single-atom sites behave differently than the clusters of the same atoms by promoting CO formation in presence of hydrogen.[14] Herein, we investigate the promotional effect of nickel on fumed-silica supported copper catalysts for CO_2 reduction in presence of H_2. The choice of catalytic sites (Cu, and Ni) is based on their effectiveness in converting CO_2 to chemicals as evidenced in numerous reported literature.[10,19,24-28] Nickel is a well-known reforming catalyst that has been used in CO_2 methanation reaction, and recent studies indicate how single atom nickel active sites prefer CO formation as compared to C—H bond formation on nickel nanoparticles.[14] Copper on the other hand is known to have potential for a variety of products formation from CO_2 hydrogenation reaction, which includes alcohols, aldehydes, acids along with hydrocarbon and CO.[10,19,29] Various synthesis methods can be adopted to alloy copper with other elements to enhance a targeted product selectivity in the thermal, electrocatalytic, and photocatalytic routes.[10-13,19,30] Here, we chose to use a localized surface combustion synthesis technique as a novel method to synthesize Cu/fumed-SiO_2 and CuNi/fumed-SiO_2 catalysts with 1 wt% loading of the metal. A small loading of the active metal allows the combustion to be localized with low energy density combustion system distributed over the inert silica support. Combustion synthesis has gained a considerable research interest for catalysts preparation over the past decade due to the simplicity of the technique that requires only a few synthesis steps for preparing reasonably large amount of catalysts.[31-37] Primarily combustion-based techniques have been used to synthesize unsupported materials, however, more recently a shift in the direction of supported catalyst is clearly seen.[38-42] The choice of fumed-SiO_2 is based on some recent reports highlighting its role in achieving a high dispersion of active sites on the surface compared to other supports.[18] Fumed SiO_2 is widely used in industries, however, studies employing it as a catalyst support are limited, though the availability of fibrous morphology resulting in large surface area has demonstrated its potential for application in catalysis.[15,18] Here we utilize fumed-SiO_2 as an inert oxide surface to perform localized combustion synthesis of Cu and CuNi active sites for CO_2 thermal reduction in a flow reactor.

2 | EXPERIMENTAL TECHNIQUES

A catalyst consisting 1 wt% of Cu and 1 wt% of CuNi (Cu = 0.5 wt%, Ni = 0.5 wt%) over fumed silica support was synthesized using surface combustion synthesis technique. The catalysts were synthesized on the basis of a 3 g batch, which is sufficient to perform catalytic tests and structural characterizations. A known amount of metal nitrate precursors ($Cu(NO_3)_2{\cdot}6H_2O$ and $Ni(NO_3)_2{\cdot}6H_2O$ both from BDH Chemicals Ltd., ~98% pure) were dissolved in deionized water (DIW, 20 mL per g of SiO_2). Then an equivalent amount of urea was added to the solution corresponding to a fuel to oxidizer ratio (φ, defined elsewhere[34,43,44]) of 1, and thoroughly mixed. Thereafter a pre-calculated amount of fumed-silica (from Alfa Aesar, amorphous fumed Silicon [IV] oxide) is added to the solution and the entire mixture, consisting of fumed silica, metal nitrates, and urea, was placed in a

crucible and inside a tubular furnace for combustion in an inert atmosphere. The tubular furnace was set at 400°C and a constant flow of 30 sccm of N_2 was maintained for 1 hour to complete the combustion resulting in the synthesis of metal supported on fumed-SiO_2. Thereafter the as-synthesized powders were collected, hand-ground and pelletized using a hydraulic-press to obtain uniform pellets with 0.6-1 mm size for assessing the catalytic properties. The Weisz-Prater criteria were used to confirm that the reaction is not diffusion-limited.[45-48] The details of calculations are provided in the supporting information. The supported catalysts were used directly for catalytic properties evaluation, without any activation/reduction in hydrogen as the synthesis conditions were maintained to get metallic/bimetallic form of copper and nickel.

The carbon dioxide conversion reaction was completed in a tubular flow reactor, BTRS-JR reactor system from Autoclave Engineers with the inner diameter of the reactor being 0.8 cm. A total of 1 g of pelletized supported catalyst was loaded inside the reactor, and a 70 sccm (CO_2 = 5 sccm, H_2 = 20 sccm, He = 45 sccm) flow rate of the reaction mixture, CO_2:H_2 of 1:4, was maintained while raising the temperature from 50°C to 650°C and maintaining a total pressure of 1 atm. These conditions result in a catalytic bed height of 3.95 cm. The reactor effluent is passed through a condenser unit, where water and other condensable products are removed, and the gases are sent to a gas chromatograph (GC, Agilent Technologies 7890A) for further analysis. The GC consisted of a Carboxen 1010 PLOT column for the separation of expected gases (such as CO, CO_2, H_2, CH_4) and a thermal conductivity detector (TCD) for a quantitative analysis of the gaseous stream. The stability of the catalysts was investigated at 650°C for ~42 hours at ambient pressure. The following definitions were used in our calculation of CO_2 conversion and CH_4 and CO yield (or conversion of CO_2 to CH_4 and CO) respectively:

$$\mathrm{CO_2\ conversion}: X_{\mathrm{CO_2}} = \frac{\mathrm{CO_{2,in}} - \mathrm{CO_{2,out}}}{\mathrm{CO_{2,in}}}, \tag{3}$$

$$\mathrm{CH_4\ yield}: Y_{\mathrm{CO_2}} = \frac{\mathrm{CH_{4,out}}}{\mathrm{CO_{2,in}}}, \tag{4}$$

$$\mathrm{CO\ yield}: Y_{\mathrm{CO}} = \frac{\mathrm{CO_{out}}}{\mathrm{CO_{2,in}}}. \tag{5}$$

The activation energy calculations were performed at low conversion (<15%) for both catalysts. The reaction rate data were obtained at three different temperature values while maintaining the same flow rate and concentration of the reactants. The reaction rates were calculated by multiplying the CO_2 molar inflow by CO_2 conversion divided by the moles of the metal content in the catalyst to get the reaction rate in [moles of CO_2 converted]/h/[moles of metal]. Arrhenius plot was obtained by plotting the logarithmic value of reaction rate with the inverse of temperature (in Kelvin) and fitting a straight line. The slope of the straight line was multiplied by the universal gas constant to get the activation energy values, as in Equation (6).

$$\ln(R) = -\frac{E_{\mathrm{act}}}{R_0}\left(\frac{1}{T}\right) + \ln(k_0 \cdot f(C)), \tag{6}$$

where R represents the reaction rate, E_{act} is the activation energy, R_0 is the universal gas constant, k_0 is the pre-exponential factor and $f(C)$ represents the concentration-dependent term in the rate law.

The fresh catalyst after synthesis, as well as the used catalysts after the stability tests was characterized for their structural and physio-chemical properties. The details of experimental conditions used during the characterization are discussed elsewhere,[23-29,49] and only a brief summary is provided here. PANalytical EMPYREAN X-ray diffractometer (XRD) was utilized to perform the XRD analysis of the samples within a 2θ range of 10° to 90° as well as to perform the low angle XRD within $2\theta < 5°$. AimSizer machine (model AS-3012) was employed to measure the total BET surface area and distribution of pore size using liquid nitrogen to provide isothermal conditions. The morphological analysis was conducted using a field emission scanning electron microscope (FESEM, Philips, XL-30) equipped with an energy dispersive X-ray spectrometer (EDX). The composition of the as-synthesized catalysts was investigated using inductively coupled plasma mass spectroscopy (ICP-MS, using NexION 300D, PerkinElmer, USA), whereas a transmission electron microscope (TEM, FEI Tecnai G2 TF20) was used for further morphological analysis.

The catalysts were assessed for their reducibility by temperature-programmed reduction (TPR) technique with H_2 (50 sccm at STP of 10% H_2 in Ar with temperature ramp of 10°C/min, approx. 0.043 g catalyst) using Micromeritics AutoChem 2950 system. Prior to the TPR experiments, the catalysts were treated at 750°C in the open air for 3 hours. The experimentally obtained TPR data were further treated using OriginLab software to correct the baseline and get the quantitative information. The hydrogen uptake in TPR profile is calibration using a standard Ag_2O reference sample. In addition, in situ FTIR (in DRIFTS mode) studies were conducted over the catalysts surface in presence of the reactive gases using Thermo-Nicolet 6700 FTIR between 50°C and 450°C. A praying-mantis optical assembly and a DRIFTS reaction

cell (both accessories from Harrick-Scientific) were used to focus the IR beam and conduct the catalytic reaction, respectively. For DRIFTS analysis, the supported catalysts were hand-ground and screened to get smaller particles with size <106 μm, which were placed in the catalyst holder and gently pressed to obtain a visually flat surface. The reactor was heated in presence of N_2 to collect background spectra at different temperatures and then cooled down to 50°C to start the DRIFTS experiments. The reaction gas mixture ($CO_2 + H_2$) was introduced and the temperature was gradually raised from 50°C to 450°C and the reaction spectra were recorded with temperature to formulate a reaction mechanism explaining the observed products.

3 | RESULTS AND DISCUSSION

The catalysts were synthesized with a fuel/oxidizer ratio of $\varphi = 1$ inside a tubular furnace in an inert atmosphere to ensure the synthesis of metallic phases rather than oxides. The synthesized catalysts as well as the used catalysts after the reaction were analyzed using XRD to identify the synthesized phases as shown in Figure 1. In case of Cu/fumed-SiO_2 synthesis, the crystalline peaks are not clearly visible except for a broad peak associated with fumed silica at 21.6°. This could be because of low loading of just 1 wt% of Cu on the support, however, zooming in around 2θ value of 40° to 70° indicates a small peak around 43.2° corresponding to the (111) crystal plane of Cu (JCPDS# 04-0836) in both the fresh and used catalysts. There is no apparent change in the XRD structure of the fresh and used Cu/fumed-SiO_2 catalyst which indicates the robustness of the catalyst and stable performance for CO_2 conversion reaction, though the low loading of 1 wt% makes it difficult to notice any structural changes if they exist. The XRD profile for CuNi/fumed-SiO_2 (Figure 1B) is much clear with evident peaks at ~43.6° and ~50.9°, closely match with the (111) and (200) crystal planes of CuNi bimetallic phase (JCPDS# 65-9048). A broad peak at 21.6° corresponding to fumed-SiO_2 is also present as in case of Figure 1A for Cu/fumed-SiO_2 samples. There are no visible changes in the crystal structure of the used catalyst, which points to the stable nature of CuNi/fumed-SiO_2 catalyst for the CO_2 reduction reaction. Small angle XRD (SAXRD) results shown in Figure S1 also indicate a very similar profile for both the samples before and after the reaction. Slight deflections are noticeable at 2θ values of 0.9° and 1.8° aligning with the (100) and (200) planes of hexagonal SiO_2 structure.[50-52] The composition of the catalyst after synthesis was further identified using ICP-MS analysis. The Cu/SiO_2 catalyst indicated 0.014 g of copper per gram of sample, whereas CuNi/SiO_2 indicated 0.007 g Cu and 0.007 g Ni per gram of the sample, respectively. So the total amount of metal content in both the samples is approx. 1.4 wt% as compared to the targeted 1 wt%. This change perhaps could be due to the loss of some SiO_2 during combustion process, as it is anticipated that some of the particles will fall out of the crucible during the sudden exothermic combustion reaction that releases a significant amount of gaseous products.

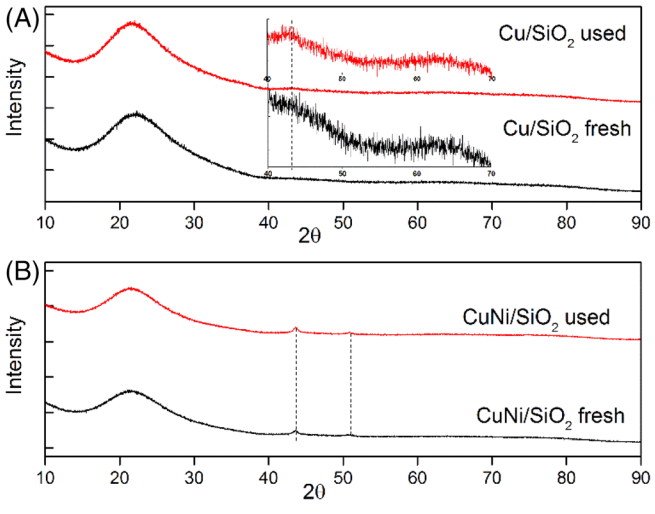

FIGURE 1 XRD pattern of fresh and spent catalysts; (A) Cu/fumed-SiO_2 and (B) CuNi/fumed-SiO_2

The SEM images of as-synthesized as well as the used samples are provided in Figure 2. Looking at the fresh catalysts in Figure 2 (A, Cu/fumed-SiO_2 and C, CuNi/fumed-SiO_2), it is clear that both the catalysts have similar and highly porous structures. This could be due to the dominating effect of SiO_2 which constitutes 99 wt% of the total sample. Fumed SiO_2 is known for its fibrous and porous characteristics that make it suitable for various industrial applications. As it is synthesized using flame combustion of silicon tetrachloride,[53] a finely dispersed and fluffy structure emerges as compared to the co-precipitated silica, which has been utilized recently in synthesizing highly dispersed active sites for different catalytic applications.[15,18] The SEM images of used catalysts after the reaction show no visible changes to the structure as shown in Figure 2B,D for Cu/fumed SiO_2 and CuNi/fumed-SiO_2 respectively. The highly porous structure is still maintained as in the fresh catalysts. TEM analysis was conducted on the synthesized samples to further analyze the structure. As shown in Figure 2E,F, both the samples show highly porous and similar structures, presumably due to high concentration of SiO_2 phase. These observations are in coherence with the XRD results discussed earlier in Figure 1, where no apparent

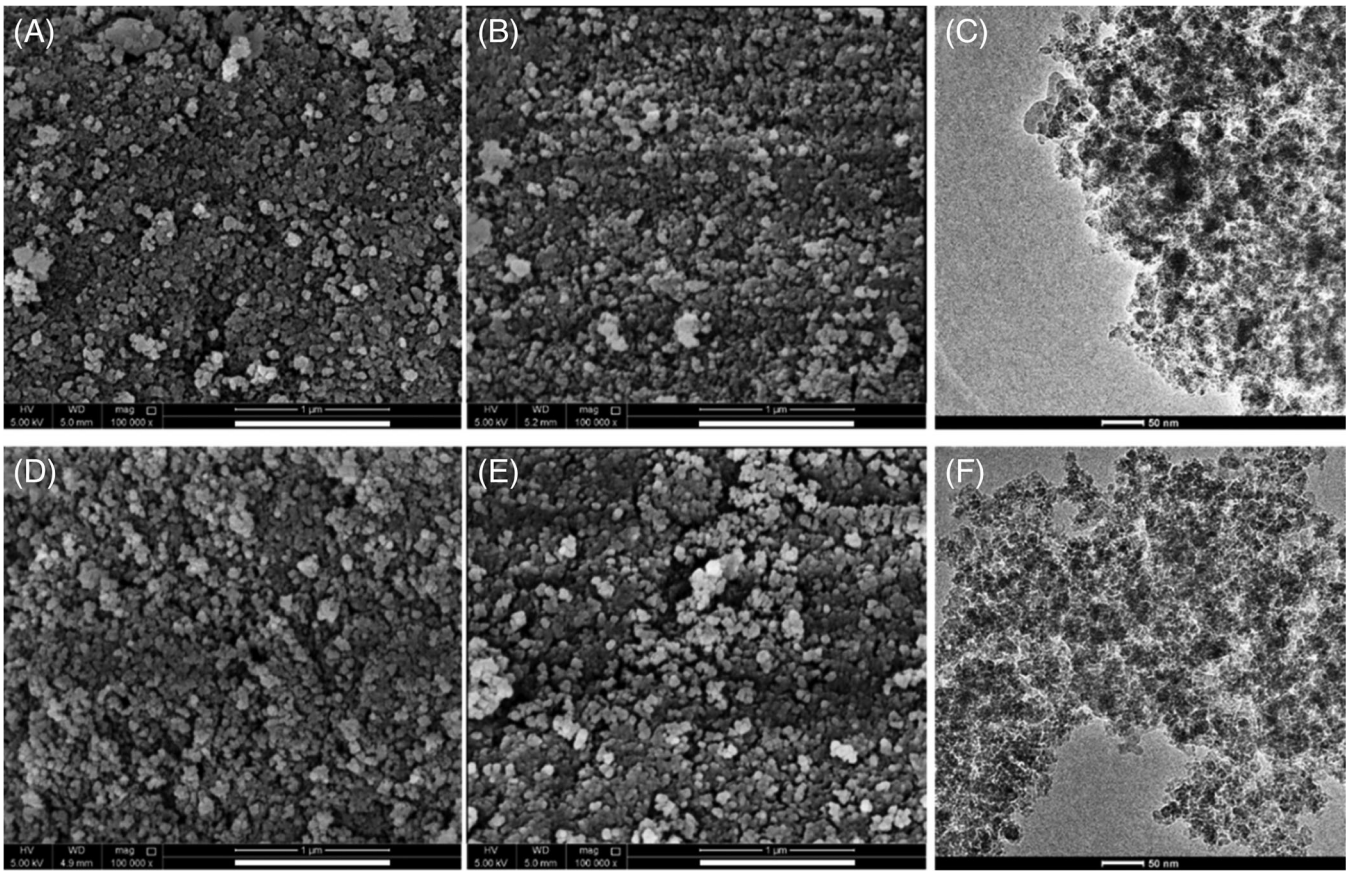

FIGURE 2 SEM microstructure images: (A) Cu/SiO_2 fresh, (B) Cu/SiO_2 used, (C) $CuNi/SiO_2$ fresh, and (D) $CuNi/SiO_2$ used. Scale bar = 1 μm; TEM images of the synthesized samples: (E) Cu/SiO_2 scale bar = 50 nm, (F) $CuNi/SiO_2$ scale bar = 50 nm

change to the crystalline structure is observed. XRD and SEM analysis together indicate that the reaction environment with temperature up to 650°C does not create any adverse impact on the catalyst, which becomes evident in our analysis of the CO_2 conversion reaction. The EDX elemental analysis of the samples was also conducted before and after the reaction as presented in Table S1. As shown, there is not much change in the composition after the reaction. No carbon was identified in any of the samples before and after the reaction.

The two catalysts were evaluated for their performance for CO_2 conversion reaction in a tubular flow reactor. The details of reaction conditions are provided in the experimental section. Figure 3A shows the conversion of carbon dioxide as a function of temperature over a range of 50°C to 650°C. Both the catalysts show activity for CO_2 conversion reaction with CuNi/fumed-SiO_2 being more active than Cu/fumed-SiO_2, throughout the temperature range. Both the catalysts start to show an exponential increase in conversion from temperature around 250°C, with 50% conversion temperature, T_{50}, being 550°C and 607°C for CuNi/fumed-SiO_2 and Cu/fumed-SiO_2 respectively, with the former showing approx. 57°C lower temperature to achieve 50% conversion of CO_2. Their conversion seems to merge at higher temperature of around 650°C with values being 61% and 60% for CuNi/fumed-SiO_2 and Cu/fumed-SiO_2 respectively, close to the thermodynamic equilibrium conversion.[54] Figure 3B shows the product yield for the two catalysts, with Cu/fumed-SiO_2 being exclusively selective for CO and no trace of CH_4 is seen up to 650°C temperature. CuNi/fumed-SiO_2 on the other hand shows a good selectivity for CO, however between 400°C and 650°C methane formation is also observed, nonetheless CO yield is always higher than CH_4 throughout the entire temperature range of this study. Methane formation starts around 400°C and reaches a maximum yield of 8.5% at 500°C and thereafter gradually decreases to zero at 650°C. The addition of Ni helps in methanation process by promoting the C—H bond formation as it is a well-known catalyst for CO and CO_2 methanation reaction.[15,25,55,56] Thermodynamically, a higher conversion of CO_2 at low temperatures (50°C) is possible, with selectivity towards more stable hydrocarbons (eg, CH_4) rather than CO, which is selective at higher temperatures only,[54,57] however, in presence of catalysts we do not see any methane

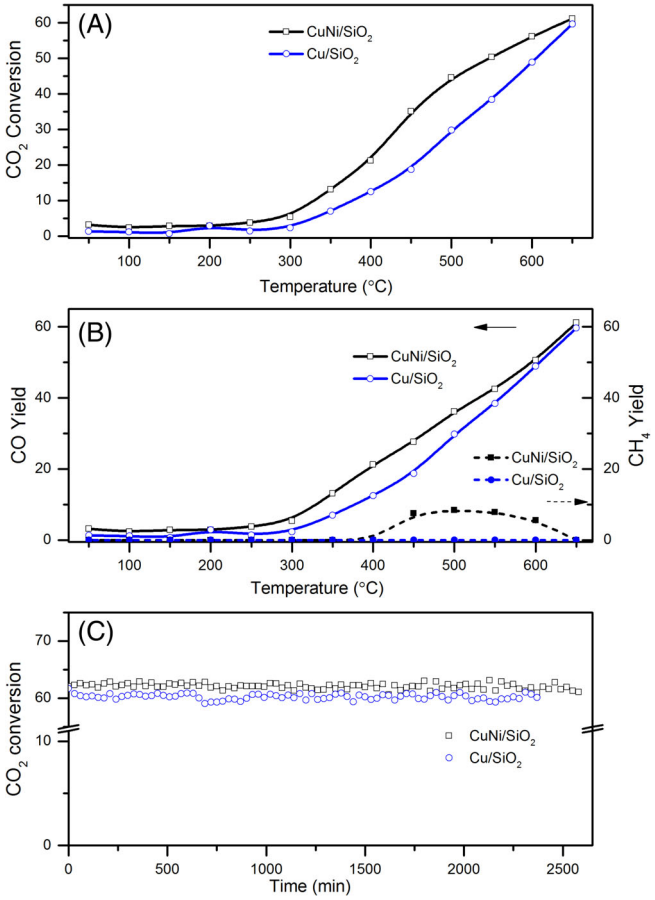

FIGURE 3 Catalytic performance of Cu/fumed-SiO_2 and CuNi/fumed-SiO_2; (A) activity, (B) yield for CO and CH_4, and (C) stability

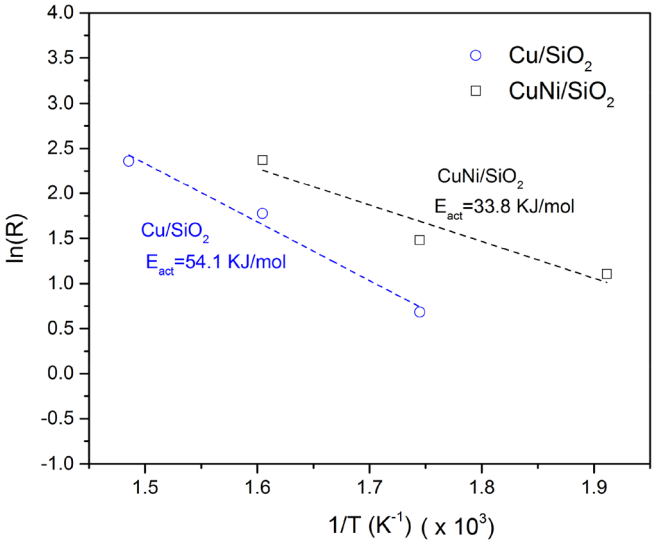

FIGURE 4 Activation energy calculation for CO_2 conversion reaction over Cu/fumed-SiO_2 and CuNi/fumed-SiO_2

formation at a temperature below 400°C and only CO as a product is observed. It should be noted that the thermodynamic calculations are performed under simplified assumptions such as homogeneous phases, and gaseous compounds following ideal gas laws, etc. The catalytic reaction environment could be significantly different involving multiple phases and interaction among non-ideal gases, leading to product distribution different from projected thermodynamic calculations. The catalysts were further evaluated for their stability towards CO_2 conversion reaction at 650°C for approx. 42 hours TOS. As shown in Figure 3C, both Cu/fumed-SiO_2 and CuNi/fumed-SiO_2 showed stable performance without any deactivation. The XRD and SEM images provided in Figures 1B and 2B,D belong to the used catalysts after the stability analysis; and the structure remains intact without showing any sign of agglomeration or deformation in the porous morphology.

The rate of reaction and activation energies were calculated at low conversion conditions (<15%) for the two catalysts. The parameters used for the calculation of activation energy (eg, temperature, conversion, and corresponding reaction rates) are provided in Table 1. As shown in Figure 4, the addition of Ni helps in decreasing the activation barrier and thereby accelerates the reaction at a relatively lower temperature. The activation energy for Cu/fumed-SiO_2 was calculated to be 54.1 kJ/mol, whereas for CuNi/fumed-SiO_2, the value was found to be only 33.8 kJ/mol. From the reaction rate calculations at low CO_2 conversion values, it is clear that the addition of Ni helps almost double the rate of reaction. As shown in Table 1, the reaction rate values are 4.4 $mol_{CO_2}/h/mol_{metal}$ and 10.7 $mol_{CO_2}/h/mol_{metal}$ at 300°C and 350°C for CuNi/fumed-SiO_2 as compared to 1.98 $mol_{CO_2}/h/mol_{metal}$ and 5.91 $mol_{CO_2}/h/mol_{metal}$ for Cu/fumed-SiO_2 for the same temperature values.

TPR studies were used to obtain the reducibility profiles of the catalysts, and to understand the impact of Ni addition on the reducibility characteristics of Cu/fumed-SiO_2 catalyst. As the results indicate in Figure 5, Cu/fumed-SiO_2 shows a broad peak at 249°C for the reduction of copper oxides to copper. The peak was further deconvoluted resulting in a combination of two peaks, which correspond to a high-intensity peak at 249°C and a low-intensity peak at 322°C. The lower temperature peak is related to finely dispersed copper oxide phase, whereas the high-temperature peak is normally linked to the bulk nanoparticle phases or copper oxides confined in micro-pores of silica that are difficult to reduce.[58-60] As the intensity trend indicates, Cu/fumed-SiO_2 primarily consists of highly dispersed copper phases that form the active sites responsible for catalytic conversion of CO_2 to CO.

TABLE 1 Activation energy calculation parameters

	CO_2 conversion (%)		Reaction rate (mol-CO_2/h/mol-metal)	
Temperature (°C)	Cu/fumed-SiO_2	CuNi/fumed-SiO_2	Cu/fumed-SiO_2	CuNi/fumed-SiO_2
250	-	3.7		3.03
300	2.3	5.4	1.98	4.4
350	7	13.1	5.91	10.7
400	12.4	-	10.59	

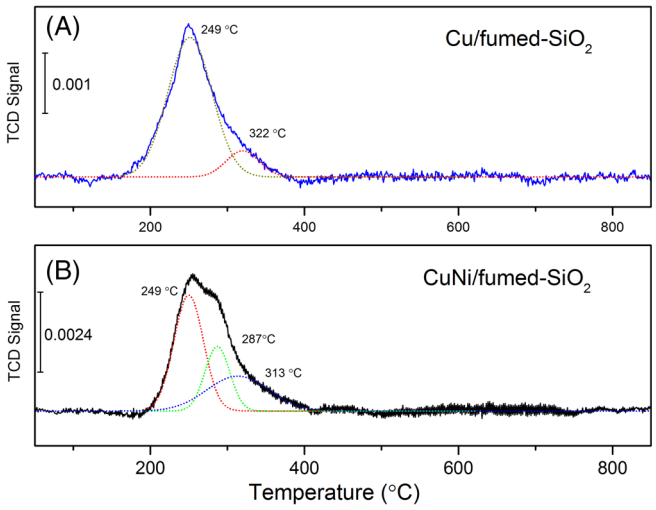

FIGURE 5 TPR profiles for: (A) Cu/fumed-SiO_2 and (B) CuNi/fumed-SiO_2

Figure 5B shows the TPR result of CuNi/fumed-SiO_2 to illustrate the effect of nickel incorporation in the catalyst. A deconvolution of the TPR profile shows the presence of three different peaks at 249°C, 287°C, and 313°C, with gradually decreasing intensity. The H_2-consumption corresponding to 249°C has clearly increased significantly in presence of Ni, which indicates a better dispersion of the copper sites. According to the literature, the low-temperature peaks indicate well dispersed active sites that could be composed of oxides of copper and nickel, whereas the high-temperature peak represents sites that are difficult to reduce.[61-63] It is well known that nickel improves the reducibility and dispersion of copper,[62,63] and interfacing copper with silica is also reported to enhance catalytic properties of copper.[64] These two factors are combined here to generate a highly dispersed active phase. Addition of nickel results in a 4-fold increase in H_2 update with values of 0.89 cc/g (∼40 μmol/g) and 3.516 cc/g (∼157 μmol/g) for Cu/fumed-SiO_2 and CuNi/fumed-SiO_2 respectively. Assuming 1 mole hydrogen uptake to be equivalent to 1 mole of the metal (Cu or Ni), the dispersion of metals can be calculated to be 25.2% and 95.8% respectively for the two catalysts, indicating approximately four times increase in the metal dispersion in presence of nickel. The higher dispersion and lower activation energy justify the improvement in the catalytic activity of CuNi/fumed-SiO_2 as observed in Figure 3. In addition to high metal dispersion, the CuNi/fumed-SiO_2 catalyst also displayed a slightly higher BET surface area compared to the Cu/fumed-SiO_2 catalyst, with values being 574.9 m^2/g and 499.2 m^2/g for the two catalysts respectively. The pore volumes on the other hand were very similar with 3.45 cc/g and 3.21 cc/g for CuNi/fumed-SiO_2 and Cu/fumed-SiO_2 catalysts. Nature of the active sites, high metal dispersion as well as improved BET area could have all contributed positively in improving the CO_2 conversion activity of CuNi/fumed-SiO_2 catalyst. The CO_2 activity of our catalysts are compared with selected Cu and Ni based catalysts as presented in Table 2.

Figure 6 shows the results of DRIFT studies on Cu/fumed-SO_2 and CuNi/fumed-SiO_2 catalysts. A schematic of the reaction pathway on the two catalysts is also provided in Figure 7. The two sharp peaks around 2360 cm^{-1}, present in both the catalysts at all the investigated temperature values belong to the CO_2 molecule adsorbed on the active sites. The peak around 3740 to 3750 cm^{-1} is stronger at lower temperature and gradually decreases with an increase in temperature, correspond to O—H bond. The presence of peaks between 2850 and 2970 cm^{-1} confirms the formation of formate species, with peaks related to C—H stretching and bending modes.[65-67] As these peaks are present in both Cu/fumed-SiO_2 and CuNi/fumed-SiO_2, even though at low intensities, the catalyst surface is active at 50°C itself. The peak around 1650 cm^{-1} is also associated with the CO stretching in formates.[15] For temperature ≤100°C, both the catalysts show the presence of carbonate species (between 1000 and 1670 cm^{-1}) attached to the surface that disappear as the temperature is increased.[68,69] The emergence of peak around 2014 cm^{-1} could be associated with the linearly adsorbed CO intermediate on the surface of the catalyst,[15,70] which desorbs from the surface as a stable gas-phase product on Cu/fumed-SiO_2 surface. On

TABLE 2 Selected Cu and Ni based catalysts for CO_2 hydrogenation

Catalyst	Conversion (T_{50} = temperature for 50% conv.)	References
Cu/SiO_2	60% at 650°C T_{50} = 607°C	This work
$CuNi/SiO_2$	61% at 650°C T_{50} = 550°C	This work
Cu/CeO_2 and Cu/SiO_2	18% at 300°C for Cu/CeO_2, 6% at 300°C for Cu/SiO_2	71
Cu/CeO_2-nanorod	~50% at 450°C	72
Cu/β-Mo_2C	~48% at 600°C	73
La-doped Ni/γ-Al_2O_3	3%-15% conversion, up to 500°C	74
Ni/Cu	<50% up to 527°C	75
$Ni/nSiO_2$ (nano-sphere)	~65% conversion at 650°C	76
Ni/m-SiO_2	Max 80% at 400°C for Ni-I/m-SiO_2 and ~65% at 600°C T_{50} = 350°C	77

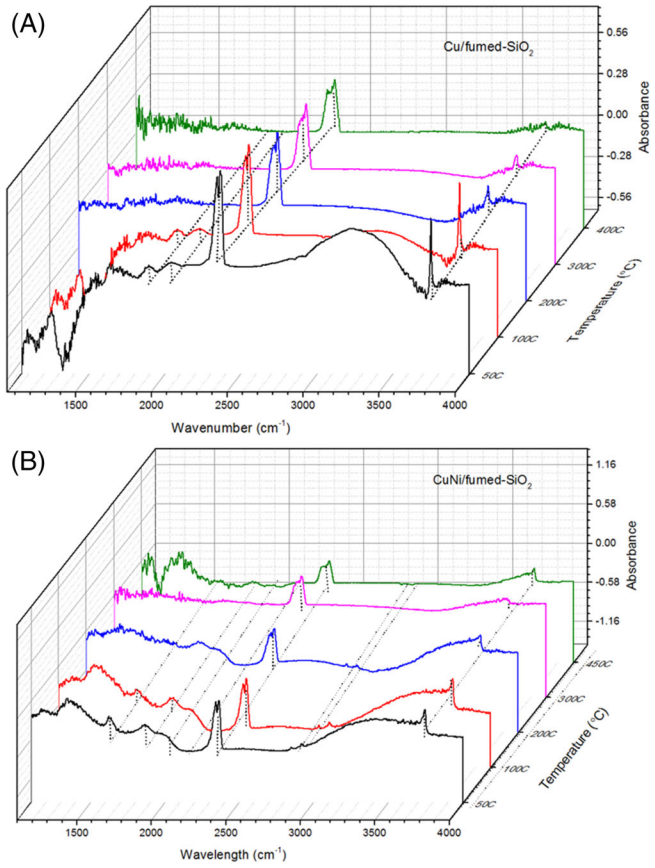

FIGURE 6 In situ DRIFT studies on (A) Cu/fumed-SiO_2 and (B) CuNi/fumed-SiO_2

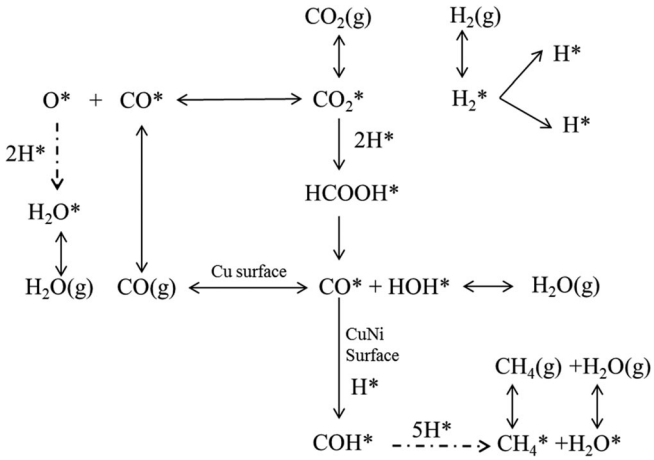

FIGURE 7 Proposed reaction pathway on Cu/fumed-SiO_2 and CuNi/fumed-SiO_2 surface

the CuNi/fumed-SiO_2 surface, a weak peak around 3020 cm^{-1} emerges at 450°C, which provides support for the formation of CH_4, possibly by successive associative reaction between adsorbed CO and adsorbed H, that is followed by the release of H_2O molecule as shown in Figure 7. Similar reaction pathways have been reported by other authors on Cu and Ni supported catalysts.[28,71] The formation of formate/carbonate intermediates are reported to precede CO formation, however, a direct splitting of the adsorbed CO_2* to adsorbed CO and adsorbed O cannot be completely ruled out.[28] The formate and carbonate intermediates have been reported to temperatures as low as 30°C to 150°C on Cu/CeO_2 and Cu/SiO_2 catalysts.[71]

4 | CONCLUSION

The effect of nickel incorporation on catalytic properties of Cu/fumed-SiO_2 catalyst for CO_2 hydrogenation reaction was investigated. The catalysts were synthesized (1 wt% Cu/fumed-SiO_2 and 1 wt% CuNi/fumed-SiO_2 [Cu = 0.5 wt%, Ni = 0.5 wt%]) using a localized surface combustion synthesis technique, where a low concentration of metal precursors in presence of an active fuel ensures the combustion to take place on the surface of fumed-SiO_2 support. Both the catalysts were active and stable for CO_2 hydrogenation reaction, with CuNi/fumed-SiO_2 showing more activity than Cu/fumed-SiO_2. Both the catalysts showed selectivity for CO at lower temperature, and some CH_4 production was also observed in presence of nickel. The TPR results indicate a higher dispersion of the metals in presence of nickel. The metal dispersion increased almost four times when nickel was introduced leading to the availability of a large number

of active sites, as well as a decrease in the activation energy for CO_2 hydrogenation reaction. DRIFTS studies indicate the formation of a formate and OH species on the surface that gradually decomposes and release CO and H_2O at elevated temperatures. Formation of CO via direct splitting of adsorbed CO_2 is also possible. The surface CO intermediate successively reacts with the neighboring H species to form methane in presence of nickel at a temperature above 400°C.

ACKNOWLEDGEMENTS

This publication was made possible by NPRP grant (NPRP8-509-2-209) from the Qatar National Research Fund (a member of Qatar Foundation). The statements made herein are solely the responsibility of the authors. The authors also gratefully acknowledge the Center for Advanced Materials (CAM) at Qatar University for services related to XRD analysis. The SEM and TEM analyses were accomplished in the Central Laboratory Unit, Qatar University, and the authors greatly appreciate their assistance in the characterization of the samples. Open Access funding provided by the Qatar National Library.

CONFLICT OF INTEREST

The authors declare no conflict of interest.

DATA AVAILABILITY STATEMENT

The data that support the findings of this study are available from the corresponding author upon reasonable request.

ORCID

Anand Kumar https://orcid.org/0000-0002-9146-979X

REFERENCES

1. Nielsen SK, Karlsson K. Energy scenarios: a review of methods, uses and suggestions for improvement. *Int J Glob Energy Issues*. 2007;27:302-322.
2. Hansen J, Johnson D, Lacis A, et al. Climate impact of increasing atmospheric carbon dioxide. *Science*. 1981;213:957-966.
3. Anwar MN, Fayyaz A, Sohail NF, et al. CO_2 capture and storage: a way forward for sustainable environment. *J Environ Manage*. 2018;226:131-144.
4. Metz B, Davidson O, Coninck H De, Loos M, Meyer L. IPCC special report on carbon dioxide capture and storage. United States: Intergovernmental Panel on Climate Change, Geneva (Switzerland) – Working Group III; 2005.
5. Nocera DG. The artificial leaf. *Acc Chem Res*. 2012;45:767-776.
6. Barber J. Photosynthetic energy conversion: natural and artificial. *Chem Soc Rev*. 2009;38:185-196.
7. Andrews E, Katla S, Kumar C, Patterson M, Sprunger P, Flake J. Electrocatalytic reduction of CO_2 at Au nanoparticle electrodes: effects of interfacial chemistry on reduction behavior. *J Electrochem Soc*. 2015;162:F1373-F1378.
8. Spinner NS, Vega JA, Mustain WE. Recent progress in the electrochemical conversion and utilization of CO_2. *Cat Sci Technol*. 2012;2:19-28.
9. Greeley J, Jaramillo TF, Bonde J, Chorkendorff IB, Nørskov JK. Computational high-throughput screening of electrocatalytic materials for hydrogen evolution. *Nat Mater*. 2006;5:909-913.
10. Nitopi S, Bertheussen E, Scott SB, et al. Progress and perspectives of electrochemical CO_2 reduction on copper in aqueous electrolyte. *Chem Rev*. 2019;119:7610-7672.
11. Nazir R, Kumar A, Ali S, Saad MAS, Al-Marri MJ. Galvanic exchange as a novel method for carbon nitride supported CoAg catalyst synthesis for oxygen reduction and carbon dioxide conversion. *Catalysts*. 2019;9:860.
12. Nazir R, Kumar A, Saleh Saad MA, Ashok A. Synthesis of hydroxide nanoparticles of Co/Cu on carbon nitride surface via galvanic exchange method for electrocatalytic CO_2 reduction into formate. *Colloids Surf A Physicochem Eng Asp*. 2020;598:124835.
13. Nazir R, Kumar A, Ali Saleh Saad M, Ali S. Development of $CuAg/Cu_2O$ nanoparticles on carbon nitride surface for methanol oxidation and selective conversion of carbon dioxide into formate. *J Colloid Interface Sci*. 2020;578:726-737.
14. Millet M-M, Algara-Siller G, Wrabetz S, et al. Ni single atom catalysts for CO_2 activation. *J Am Chem Soc*. 2019;141:2451-2461.
15. Mohammed AAA, Saad MAHS, Kumar A, Al-Marri MJ. Synthesis of fumed silica supported Ni catalyst for carbon dioxide conversion to methane. *Greenh Gases Sci Technol*. 2020;10:715-724.
16. Pakhare D, Spivey J. A review of dry (CO_2) reforming of methane over noble metal catalysts. *Chem Soc Rev*. 2014;43:7813-7837.
17. Danghyan V, Kumar A, Mukasyan A, Wolf EE. An active and stable NiO-MgO catalysts prepared by template assisted combustion synthesis for the dry reforming of methane. *Appl Catal Environ*. 2020;273:119056.
18. Danghyan V, Novoa SC, Mukasyan A, Wolf EE. Pressure dilution, a new method to prepare a stable Ni/fumed silica catalyst for the dry reforming of methane. *Appl Catal Environ*. 2018;234:178-186.
19. Ebrahimi P, Kumar A, Khraisheh M. A review of recent advances in water-gas shift catalysis for hydrogen production. *Emergent Mater*. 2020;3:881-917.
20. Abelló S, Berrueco C, Montané D. High-loaded nickel–alumina catalyst for direct CO_2 hydrogenation into synthetic natural gas (SNG). *Fuel*. 2013;113:598-609.
21. Tada S, Ikeda S, Shimoda N, et al. Sponge Ni catalyst with high activity in CO_2 methanation. *Int J Hydrogen Energy*. 2017;42:30126-30134.
22. Aldana PAU, Ocampo F, Kobl K, et al. Catalytic CO_2 valorization into CH_4 on Ni-based ceria-zirconia. Reaction mechanism by operando IR spectroscopy. *Catal Today*. 2013;215:201-207.
23. Sengupta S, Jha A, Shende P, Maskara R, Das AK. Catalytic performance of Co and Ni doped Fe-based catalysts for the hydrogenation of CO_2 to CO via reverse water-gas shift reaction. *J Environ Chem Eng*. 2019;7:102911.
24. Saeidi S, Amin NAS, Rahimpour MR. Hydrogenation of CO_2 to value-added products—a review and potential future developments. *J CO2 Util*. 2014;5:66-81.

25. Frontera P, Macario A, Ferraro M, Antonucci P. Supported catalysts for CO_2 methanation: a review. *Catalysts*. 2017;7:59.
26. Razali NAM, Lee KT, Bhatia S, Mohamed AR. Heterogeneous catalysts for production of chemicals using carbon dioxide as raw material: a review. *Renew Sustain Energy Rev*. 2012;16:4951-4964.
27. Kho ET, Tan TH, Lovell E, Wong RJ, Scott J, Amal R. A review on photo-thermal catalytic conversion of carbon dioxide. *Green Energy Environ*. 2017;2:204-217.
28. De S, Dokania A, Ramirez A, Gascon J. Advances in the design of heterogeneous catalysts and thermocatalytic processes for CO_2 utilization. *ACS Catal*. 2020;10:14147-14185.
29. Kuhl KP, Cave ER, Abram DN, Jaramillo TF. New insights into the electrochemical reduction of carbon dioxide on metallic copper surfaces. *Energy Environ Sci*. 2012;5:7050-7059.
30. Nazir R, Khalfani A, Abdelfattah O, Kumar A, Saleh Saad MA, Ali S. Nanosheet synthesis of mixed Co_3O_4/CuO via combustion method for methanol oxidation and carbon dioxide reduction. *Langmuir*. 2020;36:12760-12771.
31. Kumar A, Miller JT, Mukasyan AS, Wolf EE. In situ XAS and FTIR studies of a multi-component Ni/Fe/Cu catalyst for hydrogen production from ethanol. *Appl Catal Gen*. 2013;467:593-603.
32. Kumar A, Ashok A, Bhosale RR, et al. In situ DRIFTS studies on Cu, Ni and CuNi catalysts for ethanol decomposition reaction. *Catal Lett*. 2016;146:778-787.
33. Kumar A. Current trends in cellulose assisted combustion synthesis of catalytically active nanoparticles. *Ind Eng Chem Res*. 2019;58:7681-7689.
34. Kumar A, Wolf EE, Mukasyan AS. Solution combustion synthesis of metal nanopowders: copper and copper/nickel alloys. *AIChE J*. 2011;57:3437-3479.
35. Wolf EE, Kumar A, Mukasyan AS. Combustion synthesis: a novel method of catalyst preparation. In: Spivey J, Han Y-F, Shekhawat D, eds. *Catalysis*. Vol 31. UK: Royal Society of Chemistry; 2019:297-346.
36. Ashok A, Kumar A, Tarlochan F. Preparation of nanoparticles via cellulose-assisted combustion synthesis. *Int J Self-Propag High-Temp Synth*. 2018;27:141-153.
37. Ashok A, Kumar A, Bhosale R, Saad MAS, AlMomani F, Tarlochan F. Study of ethanol dehydrogenation reaction mechanism for hydrogen production on combustion synthesized cobalt catalyst. *Int J Hydrogen Energy*. 2017;42:23464-23473.
38. Cross A, Kumar A, Wolf EE, Mukasyan AS. Combustion synthesis of a nickel supported catalyst: effect of metal distribution on the activity during ethanol decomposition. *Ind Eng Chem Res*. 2012;51(37):12004-12008.
39. Cross A, Miller JT, Danghyan V, Mukasyan AS, Wolf EE. Highly active and stable Ni-Cu supported catalysts prepared by combustion synthesis for hydrogen production from ethanol. *Appl Catal Gen*. 2019;572:124-133.
40. Manukyan KV, Cross A, Roslyakov S, et al. Solution combustion synthesis of nano-crystalline metallic materials: mechanistic studies. *J Phys Chem C*. 2013;117:24417-24427.
41. Varma A, Mukasyan AS, Rogachev AS, Manukyan KV. Solution combustion synthesis of nanoscale materials. *Chem Rev*. 2016;116:14493-14586.
42. Ali S, Al-Marri MJ, Abdelmoneim AG, Kumar A, Khader MM. Catalytic evaluation of nickel nanoparticles in methane steam reforming. *Int J Hydrogen Energy*. 2016;41:22876-22885.
43. Kumar A, Wolf EE, Mukasyan AS. Solution combustion synthesis of metal nanopowders: nickel-reaction pathways. *AIChE J*. 2011;57:2207-2214.
44. Kumar A, Mukasyan AS, Wolf EE. Impregnated layer combustion synthesis method for preparation of multicomponent catalysts for the production of hydrogen from oxidative reforming of methanol. *Appl Catal Gen*. 2010;372:175-183.
45. Weisz PB. Sorption-diffusion in heterogeneous systems. Part 1. General sorption behaviour and criteria. *Trans Faraday Soc*. 1967;63:1801-1806.
46. Bai PT, Manokaran V, Saiprasad PS, Srinath S. Studies on heat and mass transfer limitations in oxidative dehydrogenation of ethane over Cr_2O_3/Al_2O_3 catalyst. *Procedia Eng*. 2015;127:1338-1345.
47. Medina JC, Figueroa M, Manrique R, et al. Catalytic consequences of Ga promotion on Cu for CO_2 hydrogenation to methanol. *Cat Sci Technol*. 2017;7:3375-3387.
48. Fogler HS. *Elements of Chemical Reaction Engineering*. USA: Pearson Education; 2011.
49. Tada S, Shimizu T, Kameyama H, Haneda T, Kikuchi R. Ni/CeO_2 catalysts with high CO_2 methanation activity and high CH_4 selectivity at low temperatures. *Int J Hydrogen Energy*. 2012;37:5527-5531.
50. Zhao D, Feng J, Huo Q, et al. Triblock copolymer syntheses of mesoporous silica with periodic 50 to 300 angstrom pores. *Science*. 1998;279:548-552.
51. Pan JH, Lee WI. Derivation of cubic and hexagonal mesoporous silica films by spin-coating. *Bull Korean Chem Soc*. 2005;26:418-422.
52. Pan H, Li J, Lu J, et al. Selective hydrogenation of cinnamaldehyde with $PtFex/Al_2O_3$@SBA-15 catalyst: enhancement in activity and selectivity to unsaturated alcohol by Pt-FeO_x and Pt-Al_2O_3@SBA-15 interaction. *J Catal*. 2017;354:24-36.
53. Schaefer DW, Hurd AJ. Growth and structure of combustion aerosols: fumed silica. *Aerosol Sci Tech*. 1990;12:876-890.
54. Jia C, Gao J, Dai Y, Zhang J, Yang Y. The thermodynamics analysis and experimental validation for complicated systems in CO_2 hydrogenation process. *J Energy Chem*. 2016;25:1027-1037.
55. Aneggi E, Llorca J, de Leitenburg C, Dolcetti G, Trovarelli A. Soot combustion over silver-supported catalysts. *Appl Catal Environ*. 2009;91:489-498.
56. Italiano C, Llorca J, Pino L, Ferraro M, Antonucci V, Vita A. CO and CO_2 methanation over Ni catalysts supported on CeO_2, Al_2O_3 and Y_2O_3 oxides. *Appl Catal Environ*. 2020;264:118494.
57. Kumar A. Low temperature activation of carbon dioxide by ammonia in methane dry reforming—a thermodynamic study. *Catalysts*. 2018;8:481.
58. Zhang Y, Fei J, Yu Y, Zheng X. Study of CO_2 hydrogenation to methanol over Cu-V/γ-Al_2O_3 catalyst. *J Nat Gas Chem*. 2007;16:12-15.
59. Zhang Y, Fei J, Yu Y, Zheng X. Methanol synthesis from CO_2 hydrogenation over Cu based catalyst supported on zirconia modified γ-Al_2O_3. *Energy Convers Manage*. 2006;47:3360-3367. https://doi.org/10.1016/j.enconman.2006.01.010.
60. Guo X, Mao D, Lu G, Wang S, Wu G. Glycine–nitrate combustion synthesis of CuO–ZnO–ZrO_2 catalysts for methanol synthesis from CO_2 hydrogenation. *J Catal*. 2010;271:178-185.

61. Tu C-C, Tsou Y-J, To TD, et al. Phyllosilicate-derived $CuNi/SiO_2$ catalysts in the selective hydrogenation of adipic acid to 1,6-hexanediol. *ACS Sustain Chem Eng*. 2019;7:17872-17881.
62. Pendem S, Mondal I, Shrotri A, Rao BS, Lingaiah N, Mondal J. Unraveling the structural properties and reactivity trends of Cu-Ni bimetallic nanoalloy catalysts for biomass-derived levulinic acid hydrogenation. *Sustain Energy Fuels*. 2018;2:1516-1529.
63. Ungureanu A, Dragoi B, Chirieac A, Royer S, Duprez D, Dumitriu E. Synthesis of highly thermostable copper-nickel nanoparticles confined in the channels of ordered mesoporous SBA-15 silica. *J Mater Chem*. 2011;21:12529-12541.
64. Xu C, Chen G, Zhao Y, et al. Interfacing with silica boosts the catalysis of copper. *Nat Commun*. 2018;9:1-10.
65. Le Peltier F, Chaumette P, Saussey J, Bettahar MM, Lavalley JC. In situ FT-IR and kinetic study of methanol synthesis from CO_2/H_2 over $ZnAl_2O_4$ and Cu-$ZnAl_2O_4$ catalysts. *J Mol Catal A Chem*. 1998;132:91-100.
66. Burch R, Chalker S, Pritchard J. Formation and decomposition of formate intermediates on supported Cu catalysts exposed to CO-CO_2-H_2 mixtures: evidence for a precursor state. *J Chem Soc Faraday Trans*. 1991;87:193-197.
67. Millar GJ, Rochester CH, Howe C, Waugh KC. A combined infrared, temperature programmed desorption and temperature programmed reaction spectroscopy study of CO_2 and H_2 interactions on reduced and oxidized silica-supported copper catalysts. *Mol Phys*. 1992;76:833-849.
68. Cárdenas-Arenas A, Quindimil A, Davó-Quiñonero A, et al. Isotopic and in situ DRIFTS study of the CO_2 methanation mechanism using Ni/CeO_2 and Ni/Al_2O_3 catalysts. *Appl Catal Environ*. 2020;265:118538.
69. Bersani M, Gupta K, Mishra AK, et al. Combined EXAFS, XRD, DRIFTS, and DFT study of nano copper-based catalysts for CO_2 hydrogenation. *ACS Catal*. 2016;6:5823-5833.
70. Ye R-P, Gong W, Sun Z, et al. Enhanced stability of Ni/SiO_2 catalyst for CO_2 methanation: derived from nickel phyllosilicate with strong metal-support interactions. *Energy*. 2019;188:116059.
71. Yang S-C, Pang SH, Sulmonetti TP, et al. Synergy between ceria oxygen vacancies and Cu nanoparticles facilitates the catalytic conversion of CO_2 to CO under mild conditions. *ACS Catal*. 2018;8:12056-12066.
72. Lin L, Yao S, Liu Z, et al. In situ characterization of Cu/CeO_2 nanocatalysts for CO_2 hydrogenation: morphological effects of nanostructured ceria on the catalytic activity. *J Phys Chem C*. 2018;122:12934-12943.
73. Zhang X, Zhu X, Lin L, et al. Highly dispersed copper over β-Mo_2C as an efficient and stable catalyst for the reverse water gas shift (RWGS) reaction. *ACS Catal*. 2017;7:912-918.
74. Garbarino G, Wang C, Cavattoni T, et al. A study of Ni/La-Al_2O_3 catalysts: a competitive system for CO_2 methanation. *Appl Catal Environ*. 2019;248:286-297.
75. Wang L, Guan E, Wang Z, et al. Dispersed nickel boosts catalysis by copper in CO_2 hydrogenation. *ACS Catal*. 2020;10:9261-9270.
76. Gonçalves RV, Vono LLR, Wojcieszak R, et al. Selective hydrogenation of CO_2 into CO on a highly dispersed nickel catalyst obtained by magnetron sputtering deposition: a step towards liquid fuels. *Appl Catal Environ*. 2017;209:240-246.
77. Gac W, Zawadzki W, Słowik G, Sienkiewicz A, Kierys A. Nickel catalysts supported on silica microspheres for CO_2 methanation. *Microporous Mesoporous Mater*. 2018;272:79-91.

SUPPORTING INFORMATION

Additional supporting information may be found online in the Supporting Information section at the end of this article.

How to cite this article: Kumar A, Mohammed AAA, Saad MAHS, Al-Marri MJ. Effect of nickel on combustion synthesized copper/fumed-SiO_2 catalyst for selective reduction of CO_2 to CO. *Int J Energy Res*. 2022;46:441–451. https://doi.org/10.1002/er.6586